Visible-light-driven 3D hierarchical Bi_2S_3/BiOBr hybrid structure for superior photocatalytic Cr(VI) reduction

Said M. El-Sheikh, Ahmed B. Azzam, Ramadan A. Geioushy, Farida M. El Dars, Bahaa Ahmed Salah

PII: S0925-8388(20)33877-9

DOI: https://doi.org/10.1016/j.jallcom.2020.157513

Reference: JALCOM 157513

To appear in: *Journal of Alloys and Compounds*

Received Date: 18 August 2020

Revised Date: 6 October 2020

Accepted Date: 7 October 2020

Please cite this article as: S.M. El-Sheikh, A.B. Azzam, R.A. Geioushy, F.M. El Dars, B.A. Salah, Visible-light-driven 3D hierarchical Bi_2S_3/BiOBr hybrid structure for superior photocatalytic Cr(VI) reduction, *Journal of Alloys and Compounds* (2020), doi: https://doi.org/10.1016/j.jallcom.2020.157513.

AUTHORSHIP STATEMENT

Manuscript title **Visible-light-driven 3D hierarchical Bi_2S_3/BiOBr hybrid structure for superior photocatalytic Cr(VI) reduction**

All persons who meet authorship criteria are listed as authors, and all authors certify that they have participated sufficiently in the work to take public responsibility for the content, including participation in the concept, design, analysis, writing, or revision of the manuscript. Furthermore, each author certifies that this material or similar material has not been and will not be submitted to or published in any other publication before its appearance in the ***J. of Alloys and Compounds***.

Authorship contributions

Please indicate the specific contributions made by each author (list the authors' initials followed by their surnames, e.g., Y.L. Cheung). The name of each author must appear at least once in each of the three categories below.

Category 1

Conception and designof study: S.M. El-Sheikh, Ahmed B. Azzam, R.A. Geioushy , Farida M. El-Dars, Bahaa Ahmed Salah

acquisition of data: S.M. El-Sheikh, Ahmed B. Azzam, R.A. Geioushy , Farida M. El-Dars, Bahaa Ahmed Salah

analysis and/or interpretation of data: S.M. El-Sheikh, Ahmed B. Azzam, R.A. Geioushy , Farida M. El-Dars

Category 2

Drafting the manuscript: S.M. El-Sheikh, Ahmed B. Azzam, R.A. Geioushy , Bahaa Ahmed Salah

revising the manuscript critically for important intellectual content S.M. El-Sheikh, Ahmed B. Azzam, R.A. Geioushy , Farida M. El-Dars, Bahaa Ahmed Salah

Category 3

Approval of the version of the manuscript to be published (the names of all authors must be listed):

S.M. El-Sheikh, Ahmed B. Azzam, R.A. Geioushy , Farida M. El-Dars, Bahaa Ahmed Salah

Acknowledgements

All persons who have made substantial contributions to the work reported in the manuscript (e.g., technical help, writing and editing assistance, general support), but who do not meet the criteria for authorship, are named in the Acknowledgements and have given us their written permission to be named. If we have not included an Acknowledgements, then that indicates that we have not received substantial contributions from non-authors.

This statement is signed by all the authors (*a photocopy of this form may be used if there are more than 10 authors***):**

Author's name (typed)	Author's signature	Date
S.M. El-Sheikh	S.M. El-Sheikh	9/9/2020
Ahmed B. Azzam	Ahmed B. Azzam	9/9/2020
R.A. Geioushy	R.A. Geioushy	9/9/2020
Farida M. El-Dars	Farida M. El-Dars	9/9/2020
Bahaa Ahmed Salah	Bahaa Ahmed Salah	9/9/2020

Graphical Abstract:

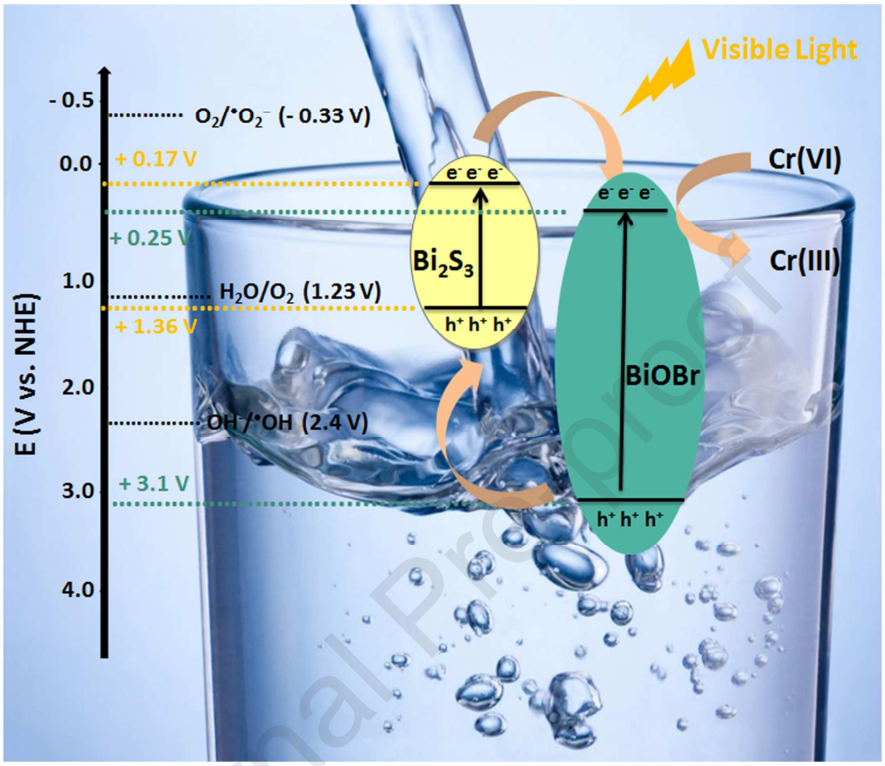

Visible-light-driven 3D hierarchical Bi_2S_3/BiOBr hybrid structure for superior photocatalytic Cr(VI) reduction

Said M. El-Sheikh[a,*], Ahmed B. Azzam[b], Ramadan A. Geioushy [a,*],

Farida M. El Dars[b], Bahaa Ahmed Salah[b]

[a] Nanomaterials and Nanotechnology Department, Advanced Materials Division, Central Metallurgical R & D Institute (CMRDI), P.O. Box, 87 Helwan, 11421 Cairo, Egypt

[b] Chemistry Department, Faculty of Science, Helwan University, Helwan, Egypt

ABSTRACT

The most important approach to eliminate poisonous Cr(VI) from water utilizing visible-light photocatalytic activities is the reduction of highly toxic Cr(VI) to less harmful Cr(III). In this study, a facile one-pot homogenous precipitation method was designed for the first time to fabricate the heterojunction of Bi_2S_3/BiOBr. The hybrid structure was characterized using XRD, FE-SEM, EDS, TEM, UV–vis (DRS), XPS, and PL. The synthesized heterostructure confirmed the successful anchoring of Bi_2S_3 nanoparticles onto BiOBr nanosheets. The as-prepared Bi_2S_3/BiOBr hybrid structure exhibited significantly enhanced photocatalytic performance for the reduction of Cr(VI) to Cr(III) compared with pure BiOBr that confirmed by XPS analysis after 10 min. The hybrid structure of Bi_2S_3/BiOBr showed a superior rate constant 10 times higher than that for pure BiOBr. Moreover, the reduction efficiency of Cr(VI) solution containing 50 mg/L was improved up to 99.2% within 40 min by the addition of tartaric acid as a hole scavenger. The reduction efficiency of different photocatalysts towards Cr(VI) removal from the real sample was also examined. The Bi_2S_3/BiOBr hybrid structure can be reused after regeneration process without a significant loss in photoreaction behavior after four recycle runs.

Keywords: Bi_2S_3/BiOBr; Hybrid structure; Photoreduction; Cr(VI)

---

* Corresponding authors.

E-mail address: selsheikh2001@gmail.com (Said M. El-Sheikh, S.M. El-Sheikh)

r_gushy@yahoo.com (Ramadan A. Geioushy, R.A. Geioushy).

1. Introduction

Heavy metals such as chromium (Cr) mainly come from waste-water of electroplating, production of steel and alloys, wood preservation, tannery, and paint area [1,2], therefore industrial discharge of chromium contaminants into water resources is becoming more serious that caused severe environmental damage [3,4]. In this regard, the US Environmental Protection Agency (EPA) listed Cr(VI) as one of the priority pollutants and very poisonous to most organisms [5], while Cr(III) is easily precipitated as $Cr(OH)_3$ and less toxic [6]. Nowadays, many efforts utilized simple and efficient techniques to remove Cr(VI) such as ion exchange, membrane separation, photoreduction to less harmful Cr(III), etc [7,8]. Photocatalytic technology plays a dominant role in solving the problems of energy crises and environmental pollution[9]. Owing to their efficiency, cost-effective, and easily applicable, photocatalysts such as TiO_2 [10,11], Bi_2WO_6 [12,13], Bi_2MoO_6 [14,15], CdS[16,17], α-Fe_2O_3[18], Ag_3VO_4 [19], ZnO [20], g-C_3N_4 [21,22], reduced graphene oxide [23], and $BiPO_4$ [24,25] have been widely used to assess the influence of environmental stressors. Bismuth-based photocatalysts are the most promising photocatalysts that achieved a significant interest due to their potential applications in semiconductors, decomposition of organic compounds, and biomedicine [26,27]. As a common metal oxyhalide, and good chemical stability, bismuth oxybromide (BiOBr) is a layered structure that has a wide band-gap (E_g = 2.90 eV) and weak absorption ability of visible light as well as the rapid recombination of e^-/h^+ pairs make its utilization inefficient [28]. Some strategies have been employed to enhance the photocatalytic activity of BiOBr including controllable synthesis[29,30], oxygen vacancies [28], doping metals[31], and hybridization with other semiconductors, such as Bi_2WO_6 [32,33], $(BiO)_2CO_3$[34], BiOI [35], β- Bi_2O_3 [36] and Z-schemeTiO_2-Au-BiOBr [37]. On the other hand, surface morphology and surface area of the photocatalyst are of great importance to improve the photoreduction efficiency. Bismuth sulfide (Bi_2S_3) has a narrow band-gap semiconductor (~1.30 eV) which has a promising candidate for pollutant removal, electrochemical energy conversion, and storage because of its electrical and optical properties [38–40]. However, there is a challenge to the use of Bi_2S_3 as an individual photocatalyst because of its fast recombination of photogenerated e^--h^+ pairs and photo-induced corrosion [41]. One of the ways to improve the separation of charge carriers is to combine Bi_2S_3 with a

semiconductor of appropriate band position such as ZnO and BiOCl [38,42]. Sang et al. constructed nanoflower-like Bi_2O_3/Bi_2S_3 heterojunctions via a one-step hydrothermal method for Cr(VI) removal [43]. The related report on anchoring Bi_2S_3 onto BiOBr to construct Bi_2S_3/BiOBr heterostructure is still very limited. Creating of effective, simple and template-free methods for fabricating Bi_2S_3/BiOBr heterostructure remains a key research challenge for nanotechnology applications. The most common methods employed in Bi_2S_3/BiOBr heterostructure syntheses are the hydrothermal method that requires high temperatures, an extended heating period, and inert atmospheres. In this study, a facile one-pot homogenous precipitation approach was developed to prepare a hierarchical Bi_2S_3/BiOBr hybrid structure under the ambient environment for the first time. Although the previous studies reported the hydrothermal and solvothermal methods for the preparation of Bi_2S_3/BiOBr [44–46], the present work shows a facile one-step homogenous precipitation approach of Bi_2S_3/BiOBr with nanosheets hierarchically structured. This synthetic process is simple and environmentally friendly. The previous reports on Bi_2S_3/BiOBr photocatalysts have been utilized primarily for dye degradation of Rhodamine B (RhB), methyl orange (MO) and Cr(VI) reduction under visible-light irradiation but the photocatalytic activity is still unsatisfying. Significantly, the hierarchical Bi_2S_3/BiOBr heterojunction showed effective reduction of Cr(VI) under visible-light illumination. Moreover, the influence of hole scavenger (e.g. tartaric acid) has a vital role in enhancing the activity of reactions as demonstrated in this study. The kinetics and mechanism of hierarchical Bi_2S_3/BiOBr for Cr(VI) removal were investigated. Besides, the reduction efficiency of Cr(VI) removal from aqueous solutions and real samples were also examined using different photocatalysts.

2. Experimental

All chemicals and the characterization instruments were listed in the electronic supplementary information (ESI).

2.1. Synthesis of Bi_2S_3/BiOBr composite

The Bi_2S_3/BiOBr heterostructure has been constructed through a simple homogenous precipitation route. Briefly, 2.4 g of $Bi(NO_3)_3 \cdot 5H_2O$, 0.5 g CTAB, and

1.0 g thiourea was dissolved in 50 ml HNO_3 (0.2 M) with vigorous stirring at 60 ^oC for 3h. The precipitate was centrifuged, washed with methanol, and double-distilled water several times, then dried at 90 ^oC in an electrical oven for 6h. Additionally, pure BiOBr was prepared with the same procedure above without adding thiourea. Pure Bi_2S_3 was fabricated without adding CTAB at the same condition mentioned above.

2.2. Measurement of photocatalytic activity

The photocatalytic properties of BiOBr, Bi_2S_3, and Bi_2S_3/BiOBr heterostructure was investigated for the reduction of Cr(VI) to Cr(III). To probe the visible light catalytic ability, 50 mL $K_2Cr_2O_7$ solutions at different concentrations (10, 30, 50mg/L) and 50 mg of photocatalyst material were added to each bottle and stirred in dark condition for 30 min to achieve the sorption equilibrium before light irradiation. Afterward, the halogen lamp (500 W, $\lambda > 400$ nm) was used to irradiate the suspension mixture for a certain time. A 2 mL mixture was pulled back and the suspended solid was removed by centrifugation process. The concentration of Cr(VI) has been detected using a spectrophotometer at $\lambda = 540$ nm using the diphenylcarbazide (DPZ) method [47].

3. Results and discussion

3.1. Characterization

The crystal phases of BiOBr, Bi_2S_3, and Bi_2S_3/BiOBr samples were investigated by XRD data as presented in Fig. 1. The feature patterns of Bi_2S_3 were ascribed to orthorhombic phase with JCPDS card no.17-0320. The diffraction peaks at 2-theta angles 22.3^o, 24.9^o, 28.6^o, 31.7^o, 35.5^o, and 39.8^o, which correspond to the crystal orientations of (220), (130), (211), (221), (240), and (141), planes of pure Bi_2S_3, respectively [48]. For pure BiOBr, the diffraction peaks at 2-theta angles of 25.2^o, 31.7^o, 32.2^o, 38.9^o, 46.2^o, and 57.1^o, can be indexed to the (101), (102), (110), (112), (200), and (212), planes of tetragonal BiOBr (JCPDS card no. 09-0393), respectively [33]. No other peaks or impurities were detected, indicates the pure phases. The intensity of the (102), (200) and (212) planes of BiOBr decreased after heterojunction with Bi_2S_3. Further, the diffraction peaks at (130), and (211) planes appeared in Bi_2S_3/BiOBr sample confirmed the formation of Bi_2S_3 orthorhombic phase.

Consequently, the results confirm the presence of Bi_2S_3 and BiOBr in the Bi_2S_3/BiOBr hybrid structure.

Fig. 2 shows the surface morphologies of the Bi_2S_3, BiOBr, and Bi_2S_3/BiOBr samples. The Bi_2S_3 sample displayed a microsphere shaped like urchin as shown in Fig. 2A–B. The high magnification of SEM shows that the microsphere urchin shape consists of well-arranged nanorods with a diameter 4 µm as shown in Fig. 2C. Furthermore, the BiOBr sample appeared as three-dimensional hierarchical micro-spheres architectures composed of hundreds of well-arranged nano-sheets as shown in Fig. 2 D-F. CTAB serves not only as the template but also as the Br source. As a template, CTAB are able to self-aggregate into various structures, such as cubic, hexagonal, and lamellar structure. CTAB offers robust chemical and mechanical stability that prevents the aggregation of BiOBr nanosheets. This could possibly assist in the formation of 3D hierarchical structure [49]. After the coupling of Bi_2S_3 with BiOBr, the hierarchical Bi_2S_3/BiOBr hybrid structure was formed by releasing Br^- from CTAB and S^{2-} from thiourea to react with Bi^{3+} through a homogenous precipitation route. The SEM image of Bi_2S_3/BiOBr sample revealed that the formation of BiOBr sheets with a rough surface (Fig. 2G-I). This heterojunction might be conducive to the separation of photo-induced carriers at the interface between Bi_2S_3 and BiOBr**.**

To further illustrate the heterojunction structure between Bi_2S_3 and BiOBr, the TEM image (Fig. 2J) indicates that BiOBr formed rounded and quadrate nanosheets and Bi_2S_3 nanoparticles are tightly attached on BiOBr nanosheet, indicating that Bi_2S_3 and BiOBr are successfully combined. The SAED pattern (Fig. 2K) demonstrated to be a single crystal with high crystallinity of the tetragonal phase. Fig. 2 L shows X-ray energy dispersive spectrometry (EDS) of Bi_2S_3/BiOBr sample and it can be seen from the figure that the hybrid structure contains Bi, O, Br, and S elements. Furthermore, EDS analysis indicates that the molar ratio of Bi_2S_3/BiOBr is about 0.53:1.

The valence states of Bi_2S_3/BiOBr heterojunction were further investigated by XPS analysis as presented in Fig. 3A-D. The distinct peaks in the survey spectra (Fig. 3A) evidence the co-existence of Bi, Br, S and O elements. The two peaks located at

158.82 and 164.12 eV with a separation distance of 5.3 eV are indexed to Bi $4f_{7/2}$ and Bi $4f_{5/2}$, respectively (Fig. 3B), proving the existence of Bi^{3+} in Bi_2S_3/BiOBr hybrid structure [50]. A certain parts of bismuth exist in the Bi–Br bonding appeared at two weak peaks with the binding energy of 156.32–162.72 eV that attributed to Bi $4f_{7/2}$ and Bi $4f_{5/2}$, respectively [51]. The characteristic peak at 67.32 eV is correlated to Br 3d in BiOBr (Fig. 3C) [52]. Meanwhile, the peak located at 225 eV (S 2s) can be ascribed to Bi–S species (Fig. 3D) [46]. As seen in Fig. 3E, the bands of O 1s appeared at 529.85, 531.61, and 533.6 eV are assigned to lattice oxygen O^{2-} (in Bi–O bond), and adsorbed oxygen, respectively [53].

To illustrate the optical properties of the pure BiOBr, Bi_2S_3, and Bi_2S_3/BiOBr heterostructure, UV–vis (DRS) analysis was conducted as shown in Fig. 4. Clearly, the pure BiOBr displays a week absorption ability with an absorption edge that appeared at 450 nm in the visible light region. On the other hand, the absorption band of pure Bi_2S_3 starts from the whole range of the visible light region. However, the Bi_2S_3/BiOBr heterostructure exhibits an intense absorption for visible light compared with pure BiOBr. The absorption range to the visible-light spectrum of the Bi_2S_3/BiOBr hybrid structure was improved which is ascribed to the optical properties of Bi_2S_3.

The bandgap energy (E_g) of pure Bi_2S_3, Bi_2S_3/BiOBr heterojunction, and pure BiOBr can be estimated by the following equation [54]:

$$(F(R)\, h\upsilon)^{0.5} = A(h\upsilon - E_g)$$

where $F(R)$ is diffuse reflection absorption coefficient, $h\upsilon$ is the photon energy, A is a constant , and E_g is bandgap energy. The bandgap energy for the indirect transition of Bi_2S_3, Bi_2S_3/BiOBr heterostructure, and BiOBr were approximately 1.19, 1.35, and 2.85 eV, respectively, that estimated from the plot of $((F(R)h\upsilon)^{0.5}$ versus $h\upsilon$ by extrapolating the straight line to the X- axis intercept as shown in Fig. S1. Therefore, the bandgap energy of Bi_2S_3/BiOBr hybrid structure showed a greater enhancement compared with pure BiOBr.

As illustrated in the PL spectra of pure BiOBr, and Bi_2S_3/BiOBr heterostructure (Fig. 5), the PL of photocatalysts were excited at 310 nm and emitted around 469 nm. Pure BiOBr sample showed a stronger emission peak intensity. In contrast, a weaker

emission was observed for Bi_2S_3/BiOBr sample, indicating the photogenerated charges recombination rate in Bi_2S_3/BiOBr was much lower than that of pure BiOBr due to the presence of Bi_2S_3. Therefore, Bi_2S_3/BiOBr is expected to exhibit an enhanced photoreduction efficiency for Cr(VI) removal through the efficient separation of charge carriers.

3.2. photocatalytic activity

The catalytic activity of BiOBr, Bi_2S_3, and Bi_2S_3/BiOBr hybrid structure for Cr(VI) photoreduction was carried out under visible light. As seen in Fig. 6A, Bi_2S_3 and Bi_2S_3/BiOBr photocatalysts exhibited a good performance towards Cr(VI) reduction. Obviously, Bi_2S_3 and Bi_2S_3/BiOBr performed the highest photocatalytic activities of 57.6% and 74.4% Cr(VI) removal within 60 min under visible irradiation respectively, which is better than those of BiOBr (12 %). This could be explained by the synergistic effect between BiOBr nanosheets and Bi_2S_3 nanoparticles that promote a good separation and transfer of photoinduced charge carriers.

The photoreduction kinetics was evaluated by Langmuir–Hinshelwood (L–H) relationship for the first-order model is well established as follows [55,56]:

$$\ln(C_t / C_o) = - kt$$

C_o and C_t represent the Cr(VI) concentrations at times 0 and t, respectively, and k_{app} is the apparent rate constant (min^{-1}). To estimate k_{app} value, the slope between $\ln(C_t/C_0)$ versus time (t) was calculated (Fig. 6B). The rate constants (k_{app}) of the BiOBr, Bi_2S_3, and Bi_2S_3/BiOBr hybrid structure are 0.002, 0.014, and 0.02 min^{-1}, respectively (Fig. 6C). Consequently, the Bi_2S_3/BiOBr heterojunction performed the highest efficient reduction rate constant for Cr(VI) among the as-prepared photocatalysts which is approximately 10 times in contrast with pure BiOBr. The characteristic binding energy peaks of Cr(III) are observed at 577.2 and 586.32 eV (Fig. 6D) which related to Cr $2p_{3/2}$ and Cr $2p_{1/2}$, respectively, confirming the conversion of Cr(VI) to Cr(III). The peak of Cr $2p_{1/2}$ at 588 eV and another peak of Cr $2p_{3/2}$ at 579 eV can be assigned to Cr(VI) [45].

The quantum yield of a photocatalytic reaction is defined as the number of Cr(VI) molecules being removed per photon absorbed. The rate constant of Cr(VI) under

visible light irradiation can also be calculated its reaction quantum yield according to the following equation[57]:

$$\phi = \frac{K}{2.303 \times Io\ \varepsilon\ l}$$

where ϕ is the reaction quantum yield, I_0 is the light intensity of the event light range at 200–800 nm (1.381×10^{-6}), ε is the molar absorptive of Cr(VI) at 540 nm (4.3×10^{4}), and l is the path length (1 cm) of the reaction.

In addition, the photoreduction quantum yields of BiOBr, Bi_2S_3, and Bi_2S_3/BiOBr samples are 0.014, 0.102, and 0.146 respectively. These results confirm the quantum yield of Bi_2S_3/BiOBr hybrid structure enhanced the photocatalytic performance for reduction of Cr(VI) to Cr(III) compared with pure BiOBr.

To probe the photoreduction performance of Bi_2S_3/BiOBr hybrid structure, different concentrations of Cr(VI) were used. It is clearly seen that the performance of Bi_2S_3/BiOBr tends to decrease with increasing Cr(VI) concentration as presented in Fig.7. When Bi_2S_3/BiOBr was exposed to visible light for 10 min, a complete reduction performance of 10 mg/L Cr(VI) was achieved to 98.3% (Fig. 7A). In contrast, 30 mg/L and 50 mg/L Cr(VI) solution concentration, the reduction performance reache to 74.3% and 57% within 60 min and 200 min, respectively (Fig. 7 B and 7C).

In order to study the impact of the different adding amount of thiourea on the catalytic performance of the composite during synthesis process. Different amount of thiourea (TU) with 0.5, 1.0, 2.0 g was added during preparation of Bi_2S_3 /BiOBr composite. As shown in (Fig. 7 D), the Cr(VI) reduction efficiencies are 67% at TU 0.5 g, 98% at TU 1.0 g, and 58% at TU 2.0 g, respectively. The photocatalytic reduction rate of Cr(VI) was improved with increasing amount of thiourea and then decreased. Increasing amount of thiourea produces more Bi_2S_3 that covers surface of BiOBr and decreases photocatalytic activity due to increasing recombination of photo-induced e^- and h^+ pairs.

The pH effect has been studied as shown in Fig. 7E. The reduction rate decreased rapidly with increasing the pH (98.0%, 76.0%, and 45.0% at pH=2, 4 and 6, respectively). At low pH, the surface of photocatalysts becomes highly protonated and more positive for better accumulation of $HCrO^{4-}$ ions. At higher pH, the surface of

photocatalysts becomes more negative, which tends to repel the $Cr_2O_7^{2-}$ ions and hence decreases the Cr(VI) reduction [58].

Additionally, the photocatalytic reduction performance of our photocatalyst was compared with the recently published articles dealing with reduction of Cr(VI) [2,3,5,45,58–61]. The activity described by the reduction performance is strongly influenced by factors, including the nanostructure, surface area, synthesis, light source and properties of the substrate. The results are listed in Table 1 and showed that Bi_2S_3/BiOBr hybrid structure demonstrated superior photocatalytic Cr(VI) reduction.

3.3. Effect of hole Scavenger concentration (e.g. tartaric acid)

The addition of tartaric acid (TA) in the photoreduction process is a significant parameter which is ascribed to capture hole carriers, thus further enhances the photocatalytic performance by decreasing the recombination between charges [62]. The effect of different concentrations of TA ranging from 2 to 8 mM was investigated using 50 mg Bi_2S_3/BiOBr hybrid structure in 50 mL of Cr(VI) solution (50 mg/L). As shown in Fig. 8A, The percentage of Cr(VI) ion removal enhanced the photocatalytic activity of Bi_2S_3/BiOBr in the presence of TA. It was found that increasing concentration of TA provided a more favorable reduction efficiency of Cr(VI). The presence of 2, 5, and 8 mM TA showed Cr(VI) reduction percentages of 72%, 86.4% and 99.2% within 40 min, respectively. On the other hand, the photocatalytic activity was only 47.5% in the absence of TA. Consequently, the addition of TA in reduction reactions of Cr(VI) plays an important role in improving photocatalytic performance. Fig. 8B displays the kinetics of Cr(VI) removal in the presence of different concentrations of TA which follows to the first-order behavior. The rate constant *k* (0.10 min^{-1}) on 8 mM TA was about 7.14 times more than that without TA (0.014 min^{-1}) (Fig. 8C).

3.3. Photocatalytic reduction mechanism

To clarify the mechanism of photocatalytic reduction reactions over Bi_2S_3/BiOBr photocatalyst, the band edge positions of photocatalyst were estimated on the basis of the following empirical formulas [44]:

$$E_{VB} = X - E^e + 0.5E_g$$

$$E_{CB} = E_{VB} - E_g$$

where X is the absolute electronegativity of the Bi_2S_3/BiOBr photocatalyst interface (5.27 eV for Bi_2S_3 [63] and 6.18 eV BiOBr [33]), E_g is the bandgap of the photocatalyst and E^e is the energy of free electrons on the hydrogen scale (about 4.5 eV). As shown in Fig. 9, the E_{VB} value of BiOBr (3.10 eV) is more positive than that of Bi_2S_3 (1.36 eV). Therefore, the photogenerated holes on the VB BiOBr surface will transfer to that of Bi_2S_3 through the interface in the heterojunction system. Meanwhile, the E_{CB} value of Bi_2S_3 (0.17 eV) is above that of BiOBr (0.25 eV), the photogenerated electrons on the CB of Bi_2S_3 will easily migrate to that of BiOBr and convert Cr(VI) to Cr(III) as the reduction potential of Cr(IV)/Cr(III) is 2.1 eV [64]. As illustrated in Fig. 9, the photoexcited electrons in the CB of BiOBr and Bi_2S_3 cannot reduce O_2 to $^{\bullet}O_2^-$, because the standard redox potentials of E^{Θ} ($O_2/{\bullet}O_2^-$) (−0.33 eV) is more negative than the CB potential of BiOBr and Bi_2S_3 (E_{CB} (BiOBr) = 0.25 eV, E_{CB} (Bi_2S_3) = 0.17 eV) [64,65]. The position of the standard redox potential of ($OH^-/^{\bullet}OH$, 2.40 eV) is lower than VB of Bi_2S_3 (E_{VB}, 1.36 eV), therefore, the $^{\bullet}OH$ radicals cannot be formed by the reactions of photogenerated holes at the VB of Bi_2S_3 with OH^-/H_2O [65]. Whereas the $^{\bullet}OH$ radicals may be oxidized by OH^- or H_2O due to the position of E_{VB} (3.10 eV) of BiOBr is lower than that of standard redox potential of ($OH^-/^{\bullet}OH$).

3.4. Real sample test

The effluent sample was collected from chrome plating wastewater. This sample was diluted and subjected to the removal procedure developed in the photocatalytic activity test using different photocatalysts. The experimental procedures were done as discussed in section (2.3). The applicability of $BiPO_4/Bi_2S_3$ heterojunction in our previous work [60], and Bi_2S_3/BiOBr composite in the present study are also verified using chrome plating wastewater. The obtained values are presented in Table 2. Approximately, 95% and 98.3% of Cr(VI) removal from the aqueous solution containing Cr(VI) was found using $BiPO_4/Bi_2S_3$, and Bi_2S_3/BiOBr photocatalysts, respectively, whereas it was 52.9%, 90.3% using chrome plating wastewater sample, respectively. The decrease in photocatalytic performance may be due to the presence of interfering ions and other impurities in the industrial effluent, which may cover the

active sites available for photocatalyst surface. Therefore, the photocatalytic activity of Bi_2S_3/BiOBr heterojunction was performed a superior photocatalytic Cr(VI) reduction compared to our previous work of $BiPO_4/Bi_2S_3$ heterostructure [60].

3.5. Stability evaluation

After the reduction process of Cr(VI), the hybrid structure Bi_2S_3/BiOBr photocatalyst was recollected, washed with water, and dried in an electrical oven to reuse again. The deposited Cr(III) species can be removed via simple washing of the sample with distilled water [66]. The Cr(VI) solution was added to collected photocatalyst and evaluate the stability of photocatalyst by catalytic activity. After 4 recycles, the reusability of the photocatalyst has no significant decrease in photocatalytic performance, indicating the stability of the photocatalyst as shown in Fig. 10 A. The XRD pattern of the used composite after the fourth recycle was performed as shown Fig. 10 B. The similarity in XRD patterns implied that the sample is successfully reused and stable under visible light. These results demonstrated that the Bi_2S_3/BiOBr is a promising candidate for Cr(VI) removal and reveals its potential application for environmental remediation and industries.

4. Conclusions

A facile one-step precipitation method has been developed to prepare Bi_2S_3/BiOBr hybrid structure. The heterojunction of Bi_2S_3/BiOBr exhibited an excellent photocatalytic performance compared with pure BiOBr for the reduction of hazardous Cr(VI) to Cr(III) that could be confirmed by XPS analysis. The reduction rate constant of Bi_2S_3/BiOBr hybrid structure was about 10 times higher than those of pure BiOBr. The enhanced catalytic performance of Bi_2S_3/BiOBr is attributed to the microstructure and the synergistic effect between BiOBr and Bi_2S_3, thus improves separation rates of the photogenerated electron-hole pairs. Furthermore, addition of tartaric acid as a hole scavenger enhanced catalytic activity up to 99.2% within 40 min due to minimizing the recombination between charges. The Bi_2S_3/BiOBr hybrid structure exhibited a highly efficient value of Cr(VI) removal from the real sample, with reduction performance of 90.3%. The results included in this work are promising and displayed a visible-light responsive photocatalyst that could be applicable for environmental remediation and industrial field.

Acknowledgements

This present work was supported by Central Metallurgical Research and Development Institute (CMRDI), Egypt.

References

[1] L. Chai, S. Huang, Z. Yang, B. Peng, Y. Huang, Y. Chen, Cr (VI) remediation by indigenous bacteria in soils contaminated by chromium-containing slag, J. Hazard. Mater. 167 (2009) 516–522.

[2] J. Qu, D. Chen, N. Li, Q. Xu, H. Li, J. He, J. Lu, Coral-inspired nanoscale design of porous SnS_2 for photocatalytic reduction and removal of aqueous Cr (VI), Appl. Catal. B 207 (2017) 404–411.

[3] R. Nagarjuna, S. Challagulla, R. Ganesan, S. Roy, High rates of Cr(VI) photoreduction with magnetically recoverable nano-Fe_3O_4@Fe_2O_3/Al_2O_3 catalyst under visible light, Chem. Eng. J. 308 (2017) 59–66.

[4] S.M. El-Sheikh, M. Rabbah, Novel low temperature synthesis of spinel nano-magnesium chromites from secondary resources, Thermochim. Acta 568 (2013) 13–19.

[5] X. Yuan, C. Zhou, Q. Jing, Q. Tang, Y. Mu, A. Du, Facile Synthesis of g-C_3N_4 Nanosheets/ZnO Nanocomposites with Enhanced Photocatalytic Activity in Reduction of Aqueous Chromium(VI) under Visible Light, Nanomaterials 6 (2016) 173.

[6] X.D. Du, X.H. Yi, P. Wang, W. Zheng, J. Deng, C.C. Wang, Robust photocatalytic reduction of Cr(VI) on UiO-66-NH_2 (Zr/Hf) metal-organic framework membrane under sunlight irradiation, Chem. Eng. J. 356 (2019) 393–399.

[7] C. Chang, L. Zhu, S. Wang, X. Chu, L. Yue, Novel Mesoporous Graphite Carbon Nitride/BiOI Heterojunction for Enhancing Photocatalytic Performance Under Visible-Light Irradiation, ACS Appl. Mater. Interfaces 6 (2014) 5083–5093.

[8] S.C. Yan, Z.S. Li, Z.G. Zou, Photodegradation of Rhodamine B and Methyl Orange over Boron-Doped g-C_3N_4 under Visible Light Irradiation, Langmuir 26 (2010) 3894–3901.

[9] H. Yin, Y. Cao, T. Fan, B. Qiu, M. Zhang, J. Yao, P. Li, X. Liu, S. Chen, Construction of carbon bridged TiO_2/CdS tandem Z-scheme heterojunctions toward efficient photocatalytic antibiotic degradation and Cr (VI) reduction, J. Alloys Compd. 824 (2020) 153915.

[10] T.M. Khedr, S.M. El-Sheikh, A.A. Ismail, D.W. Bahnemann, Highly efficient solar light-assisted TiO_2 nanocrystalline for photodegradation of ibuprofen drug, Opt. Mater. 88 (2019) 117–127.

[11] G. Zhang, M.N. Nadagouda, K. O'Shea, S.M. El-Sheikh, A.A. Ismail, V. Likodimos, P. Falaras, D.D. Dionysiou, Degradation of cylindrospermopsin by using polymorphic titanium dioxide under UV-Vis irradiation, Catal. Today 224 (2014) 49–55.

[12] S. Li, J. Chen, S. Hu, H. Wang, W. Jiang, X. Chen, Facile construction of novel Bi_2WO_6/Ta_3N_5 Z-scheme heterojunction nanofibers for efficient degradation of harmful pharmaceutical pollutants, Chem. Eng. J. 402 (2020) 126165.

[13] S. Li, J. Chen, S. Hu, W. Jiang, Y. Liu, J. Liu, A novel 3D Z-scheme heterojunction photocatalyst: $Ag_6Si_2O_7$ anchored on flower-like Bi_2WO_6 and its excellent photocatalytic performance for the degradation of toxic pharmaceutical antibiotics, Inorg. Chem. Front. 7 (2020) 529–541.

[14] S. Li, S. Hu, W. Jiang, Y. Liu, Y. Zhou, J. Liu, Z. Wang, Facile synthesis of cerium oxide nanoparticles decorated flower-like bismuth molybdate for enhanced photocatalytic activity toward organic pollutant degradation, J. Colloid Interface Sci. 530 (2018) 171–178.

[15] S. Li, S. Hu, W. Jiang, J. Zhang, K. Xu, Z. Wang, In situ construction of WO_3 nanoparticles decorated Bi_2MoO_6 microspheres for boosting photocatalytic degradation of refractory pollutants, J. Colloid Interface Sci. 556 (2019) 335–344.

[16] X. Xu, L. Hu, N. Gao, S. Liu, S. Wageh, A.A. Al-Ghamdi, A. Alshahrie, X.

Fang, Controlled growth from ZnS nanoparticles to ZnS-CdS nanoparticle hybrids with enhanced photoactivity, Adv. Funct. Mater. 25 (2015) 445–454.

[17] J. Fu, B. Chang, Y. Tian, F. Xi, X. Dong, Novel C_3N_4–CdS composite photocatalysts with organic–inorganic heterojunctions: in situ synthesis, exceptional activity, high stability and photocatalytic mechanism, J. Mater. Chem. A 1 (2013) 3083.

[18] S. Liu, L. Zheng, P. Yu, S. Han, X. Fang, Novel Composites of α-Fe_2O_3 Tetrakaidecahedron and Graphene Oxide as an Effective Photoelectrode with Enhanced Photocurrent Performances, Adv. Funct. Mater. 26 (2016) 3331–3339.

[19] S. Wang, Y. Guan, L. Wang, W. Zhao, H. He, J. Xiao, S. Yang, C. Sun, Fabrication of a novel bifunctional material of BiOI/Ag_3VO_4 with high adsorption-photocatalysis for efficient treatment of dye wastewater, Appl. Catal. B 168–169 (2015) 448–457.

[20] F. Kiantazh, A. Habibi-Yangjeh, Ultrasonic-assisted one-pot preparation of ZnO/Ag_3VO_4 nanocomposites for efficiently degradation of organic pollutants under visible-light irradiation, Solid State Sci. 49 (2015) 68–77.

[21] C. Lu, R. Chen, X. Wu, M. Fan, Y. Liu, Z. Le, S. Jiang, S. Song, Boron doped g-C_3N_4 with enhanced photocatalytic UO_2^{2+} reduction performance, Appl. Surf. Sci. 360 (2016) 1016–1022.

[22] Z. Li, B. Li, S. Peng, D. Li, S. Yang, Y. Fang, Novel visible light-induced g-C_3N_4 quantum dot/$BiPO_4$ nanocrystal composite photocatalysts for efficient degradation of methyl orange, Rsc Adv. 4 (2014) 35144–35148.

[23] S.I. El-hout, S.M. El-sheikh, A. Gaber, A. Shawky, A.I. Ahmed, Highly efficient sunlight-driven photocatalytic degradation of malachite green dye over reduced graphene oxide-supported CuS nanoparticles, J. Alloys Compd. 849 (2020) 156573.

[24] Q. Zhang, P. Chen, M. Zhuo, F. Wang, Y. Su, T. Chen, K. Yao, Z. Cai, W. Lv, G. Liu, Degradation of indometacin by simulated sunlight activated CDs-loaded $BiPO_4$ photocatalyst: Roles of oxidative species, Appl. Catal. B 221

(2018) 129–139.

[25] Y. Hu, Z. Jia, R. Lv, C. Fan, H. Zhang, One-pot electrochemical preparation of BiOCl/$BiPO_4$ double-layer heterojunction film with efficient photocatalytic performance, Mater. Res. Bull. 94 (2017) 222–230.

[26] P. Madhusudan, J. Ran, J. Zhang, J. Yu, G. Liu, Novel urea assisted hydrothermal synthesis of hierarchical $BiVO_4$/$Bi_2O_2CO_3$ nanocomposites with enhanced visible-light photocatalytic activity, Appl. Catal. B 110 (2011) 286–295.

[27] A.B. Azzam, S.M. El-Sheikh, R.A. Geioushy, B.A. Salah, F.M. El-Dars, A.S. Helal, Facile fabrication of a novel $BiPO_4$ phase junction with enhanced photocatalytic performance towards aniline blue degradation, RSC Adv. 9 (2019) 17246–17253.

[28] Z.Q. Wang, H. Wang, X.F. Wu, T.L. Chang, Oxygen vacancies and p-n heterojunction modified BiOBr for enhancing donor density and separation efficiency under visible-light irradiation, J. Alloys Compd. 834 (2020) 155025.

[29] Y. Liu, Y. Yin, X. Jia, X. Cui, C. Tian, Y. Sang, H. Liu, Synthesis process and photocatalytic properties of BiOBr nanosheets for gaseous benzene, Environ. Sci. Pollut. Res. 23 (2016) 17525–17531.

[30] Z. Jiang, F. Yang, G. Yang, L. Kong, M.O. Jones, T. Xiao, P.P. Edwards, The hydrothermal synthesis of BiOBr flakes for visible-light-responsive photocatalytic degradation of methyl orange, J. Photochem. Photobiol. A 212 (2010) 8–13.

[31] Z. Wei, G. Jiang, L. Shen, X. Li, X. Wang, W. Chen, Preparation of Mn-doped BiOBr microspheres for efficient visible-light-induced photocatalysis, MRS Commun. 3 (2013) 145–149.

[32] X. Ren, K. Wu, Z. Qin, X. Zhao, H. Yang, The construction of type II heterojunction of Bi_2WO_6/BiOBr photocatalyst with improved photocatalytic performance, J. Alloys Compd. 788 (2019) 102–109.

[33] J. Hu, W. An, H. Wang, J. Geng, W. Cui, Y. Zhan, Synthesis of a hierarchical

BiOBr nanodots/Bi_2WO_6 p–n heterostructure with enhanced photoinduced electric and photocatalytic degradation performance, RSC Adv. 6 (2016) 29554–29562.

[34] L. Gao, X. Li, J. Zhao, X. Zhang, X. Zhang, H. Yu, In situ preparation of $(BiO)_2CO_3$/BiOBr sheet-on-sheet heterojunctions with enhanced visible light photocatalytic activity, J. Phys. Chem. Solids 108 (2017) 30–38.

[35] L. Lin, M. Huang, L. Long, Z. Sun, W. Zheng, D. Chen, Fabrication of a three-dimensional BiOBr/BiOI photocatalyst with enhanced visible light photocatalytic performance, Ceram. Int. 40 (2014) 11493–11501.

[36] Y. Li, H. Wang, L. Huang, C. Wang, Q. Wang, F. Zhang, X. Fan, M. Xie, H. Li, Promoting LED light driven photocatalytic inactivation of bacteria by novel β-Bi_2O_3@BiOBr core/shell photocatalyst, J. Alloys Compd. 816 (2020) 152665.

[37] X. Yu, H. Qiu, B. Wang, Q. Meng, S. Sun, Y. Tang, K. Zhao, A ternary photocatalyst of all-solid-state Z-scheme TiO_2–Au–BiOBr for efficiently degrading various dyes, J. Alloys Compd. 839 (2020) 155597.

[38] A. Das Mahapatra, D. Basak, Enhanced ultraviolet photosensing properties in Bi_2S_3 nanoparticles decorated ZnO nanorods' heterostructure, J. Alloys Compd. 797 (2019) 766–774.

[39] J. Lu, Q. Han, Z. Wang, Synthesis of TiO_2/Bi_2S_3 heterojunction with a nuclear-shell structure and its high photocatalytic activity, Mater. Res. Bull. 47 (2012) 1621–1624.

[40] W. Luo, F. Li, Q. Li, X. Wang, W. Yang, L. Zhou, L. Mai, Heterostructured Bi_2S_3–Bi $_2O_3$ Nanosheets with a Built-In Electric Field for Improved Sodium Storage, ACS Appl. Mater. Interfaces 10 (2018) 7201–7207.

[41] E. Fenelon, D.-P. Bui, H.H. Tran, S.-J. You, Y.-F. Wang, T.M. Cao, V. Van Pham, Straightforward Synthesis of SnO_2/Bi_2S_3/BiOCl–$Bi_{24}O_{31}Cl_{10}$ Composites for Drastically Enhancing Rhodamine B Photocatalytic Degradation under Visible Light , ACS Omega 5 (2020) 20438–20449.

[42] J. Qiu, M. Li, J. Xu, X.F. Zhang, J. Yao, Bismuth sulfide bridged hierarchical Bi_2S_3/BiOCl@$ZnIn_2S_4$ for efficient photocatalytic Cr(VI) reduction, J. Hazard. Mater. 389 (2020) 121858.

[43] Y. Sang, X. Cao, G. Dai, L. Wang, Y. Peng, B. Geng, Facile one-pot synthesis of novel hierarchical Bi_2O_3/Bi_2S_3 nanoflower photocatalyst with intrinsic p-n junction for efficient photocatalytic removals of RhB and Cr(VI), J. Hazard. Mater. 381 (2020) 120942.

[44] Y. Cui, Q. Jia, H. Li, J. Han, L. Zhu, S. Li, Y. Zou, J. Yang, Photocatalytic activities of Bi_2S_3/BiOBr nanocomposites synthesized by a facile hydrothermal process, Appl. Surf. Sci. 290 (2014) 233–239.

[45] H. Li, F. Deng, Y. Zheng, H. Li, C. Qu, X. Luo, Visible-light-driven Z-scheme rGO/Bi_2S_3-BiOBr heterojunction with tunable exposed BiOBr (102) facets for efficient synchronous photocatalytic degradation of 2-nitrophenol and Cr(VI) reduction, Environ. Sci. Nano 6 (2019) 3670-3683.

[46] H. Jiao, X. Yu, Z. Liu, P. Kuang, Y. Zhang, One-pot synthesis of heterostructured Bi_2S_3 /BiOBr microspheres with highly efficient visible light photocatalytic performance, RSC Adv. 5 (2015) 16239–16249.

[47] Q. Yuan, L. Chen, M. Xiong, J. He, S.L. Luo, C.T. Au, S.F. Yin, Cu_2O/$BiVO_4$ heterostructures: Synthesis and application in simultaneous photocatalytic oxidation of organic dyes and reduction of Cr(VI) under visible light, Chem. Eng. J. 255 (2014) 394–402.

[48] C. Gao, H. Shen, Z. Shen, L. Sun, Influence of SnS buffer layers on the growth and properties of nanostructured Bi_2S_3 films by chemical bath deposition, Appl. Surf. Sci. 257 (2011) 4439–4442.

[49] A. Ahmad, X. Meng, N. Yun, Z. Zhang, Preparation of Hierarchical BiOBr Microspheres for Visible Light-Induced Photocatalytic Detoxification and Disinfection, J. Nanomater. 2016 (2016).

[50] M. Lu, G. Yuan, Z. Wang, Y. Wang, J. Guo, Synthesis of $BiPO_4$/Bi_2S_3 Heterojunction with Enhanced Photocatalytic Activity under Visible-Light Irradiation, Nanoscale Res. Lett. 10 (2015) 1–7.

[51] K.L. Li, W.W. Lee, C.S. Lu, Y.M. Dai, S.Y. Chou, H.L. Chen, H.P. Lin, C.C. Chen, Synthesis of BiOBr, Bi_3O_4Br, and $Bi_{12}O_{17}Br_2$ by controlled hydrothermal method and their photocatalytic properties Kun-Lin, J. Taiwan Inst Chem Eng 45 (2014) 2688–2697.

[52] D. Yuan, L. Huang, Y. Li, Y. Xu, H. Xu, S. Huang, J. Yan, M. He, H. Li, Synthesis and photocatalytic activity of g-C_3N_4/BiOI/BiOBr ternary composites, RSC Adv. 6 (2016) 41204–41213.

[53] J. Zhao, Q. Han, J. Zhu, X. Wu, X. Wang, Synthesis of Bi nanowire networks and their superior photocatalytic activity for Cr(VI) reduction, Nanoscale 6 (2014) 10062–10070.

[54] F. Feng, W. Yang, S. Gao, C. Sun, Q. Li, Postillumination Activity in a Single-Phase Photocatalyst of Mo-Doped TiO_2 Nanotube Array from Its Photocatalytic "memory," ACS Sustain. Chem. Eng. 6 (2018) 6166–6174.

[55] A. Shawky, S.M. El-Sheikh, M.N. Rashed, S.M. Abdo, T.I. El-Dosoqy, Exfoliated kaolinite nanolayers as an alternative photocatalyst with superb activity, J. Environ. Chem. Eng. 7 (2019) 103174.

[56] L. She, G. Tan, H. Ren, J. Huang, C. Xu, A. Xia, Photocatalytic and photoelectrochemical activity of N-doped $BiPO_4$ photocatalyst., RSC Adv. 5 (2015) 36642.

[57] Y.-J. Chen, C.-S. Tseng, P.-J. Tseng, C.-W. Huang, T. Wu, Y.-W. Lin, Synthesis and characterization of Ag/Ag_3PO_4 nanomaterial modified $BiPO_4$ photocatalyst by sonochemical method and its photocatalytic application, J. Mater. Sci. Mater. Electron. 28 (2017) 11886–11899.

[58] D. Xiao, K. Dai, Y. Qu, Y. Yin, H. Chen, Hydrothermal synthesis of α-Fe_2O_3 /g-C_3N_4 composite and its efficient photocatalytic reduction of Cr(VI) under visible light, Appl. Surf. Sci. 15 (2015)181–187.

[59] R. Djellabi, B. Yang, H.M. Adeel Sharif, J. Zhang, J. Ali, X. Zhao, Sustainable and easy recoverable magnetic TiO_2-Lignocellulosic Biomass@Fe_3O_4 for solar photocatalytic water remediation, J. Clean. Prod. 233 (2019) 841–847.

[60] R.A. Geioushy, S.M. El-Sheikh, A.B. Azzam, B.A. Salah, F.M. El-Dars, One-pot fabrication of $BiPO_4/Bi_2S_3$ hybrid structures for visible-light driven reduction of hazardous Cr(VI), J. Hazard. Mater. 381 (2020) 120955.

[61] C.L. X. Yuan, X. Wu, Z. Feng, W. Jia, X. Zheng, Facile Synthesis of Heterojunctioned ZnO/Bi_2S_3 Nanocomposites for Enhanced Photocatalytic Reduction of Aqueous Cr(VI) under Visible-Light Irradiation, Catalysts 9 (2019) 624.

[62] R. Djellabi, F.M. Ghorab, S. Nouacer, A. Smara, O. Khireddine, Cr(VI) photocatalytic reduction under sunlight followed by Cr(III) extraction from TiO_2 surface, Mater. Lett. 176 (2016) 106–109.

[63] Y. Yan, Z. Zhou, W. Li, Y. Zhu, Y. Cheng, F. Zhao, J. Zhou, Facile ion-exchange synthesis of urchin-shaped CdS/Bi_2S_3 heterostructures with enhanced photostability and visible light photocatalytic activity, RSC Adv. 4 (2014) 38558–38567.

[64] F. Zhang, Y. Zhang, G. Zhang, Z. Yang, D.D. Dionysiou, A. Zhu, Exceptional synergistic enhancement of the photocatalytic activity of SnS_2 by coupling with polyaniline and N-doped reduced graphene oxide, Appl. Catal. B 236 (2018) 53–63.

[65] J. Lu, Y. Wang, F. Liu, L. Zhang, S. Chai, Fabrication of a direct Z-scheme type WO_3/Ag_3PO_4 composite photocatalyst with enhanced visible-light photocatalytic performances, Appl. Surf. Sci. 393 (2017) 180–190.

[66] B. Liu, X. Liu, L. Li, J. Li, C. Li, Y. Gong, L. Niu, X. Zhao, C.Q. Sun, $ZnIn_2S_4$ flowerlike microspheres embedded with carbon quantum dots for efficient photocatalytic reduction of Cr(VI), Chinese J. Catal. 39 (2018) 1901–1909.

Table Caption

Table 1 Comparison of the photocatalytic reduction of Cr(VI) with various photocatalysts

Catalyst	Method	(Morphology/ Surface area)	Loading catalyst (mg)	Cr(VI) conc. (mg L^{-1})	Time (min)	Light source	Reduction %	Ref.
α-Fe_2O_3/g–C_3N_4	Hydrothermal	Nanoparticles, Nanosheets/ 77.58 m^2 g^{-1}	100	10	150	300 W Xe lamp	98%	[58]
rGO/Bi_2S_3–BiOBr	Solvothermal	Nanorods, Nanosheets/ 31.68 m^2 g^{-1}	100	10	120	300 W Xe lamp	95%	[45]
SPNH-MOSF@SnS_2	Hydrothermal	Nanoplates, Corallite/ 103.85 m^2 g^{-1}	50	50	90	300 W Xe lamp	99.5%	[2]
10% Fe_3O_4@Fe_2O_3 /Al_2O_3	co-precipitation	Nanoparticles/ 86.2 m^2 g^{-1}	50	50	25	250 W HPS visible lamp	100%	[3]
TiO_2-OP@Fe_3O_4	Hydrothermal	104.7 m^2 g^{-1}	50	10	40	300 W Xe lamp	100%	[59]
$BiPO_4$/Bi_2S_3	Precipitation	Cocoon, Flower/-	50	10	20	500 W halogen lamp	95%	[60]
ZnO/Bi_2S_3	Solvothermal	Nanoparticles, Nanoplates/-	50	10	120	500 W Xe lamp	95%	[61]
g-C_3N_4 /ZnO	Precipitation-calcination	Nanoparticles, Sheets/-	50	10	240	500 W Xe lamp	70%	[5]
Bi_2S_3/BiOBr	Homogenous precipitation	Nanoparticles, Nanosheets/-	50	10	10	500 W halogen lamp	98%	This work

Table 2 Removal percentage of Cr(VI) from aqueous solution and chrome plating wastewater sample.

photocatalyst	Removal percentage (%) from model aqueous solution	Removal percentage (%) from real wastewater sample	Ref.
$BiPO_4/Bi_2S_3$	95% ± 0.58	52.9% ± 2.1	[60]
Bi_2S_3/BiOBr	98.3% ± 1.2	90.3% ± 1.8	Present study

Figure Captions

Fig. 1 Powder XRD patterns of the pure Bi_2S_3, Bi_2S_3/BiOBr heterostructure, and the pure BiOBr.

Fig. 2 SEM images of the pure Bi_2S_3 (A-C), the pure BiOBr (D-F), Bi_2S_3/BiOBr heterostructure (G-I); TEM, SEAD pattern of Bi_2S_3/BiOBr heterostructure (J, K, respectively), and EDS of Bi_2S_3/BiOBr hybrid structure (L).

Fig. 3 XPS spectra for the hybrid structured Bi_2S_3/BiOBr: (A) full survey, (B) Bi 4f, (C) Br 3d, (D) S 2s, and (E) O 1s.

Fig. 4 (A) UV–Vis diffuse reflection spectrum of the pure Bi_2S_3, Bi_2S_3/BiOBr heterostructure, and the pure BiOBr.

Fig. 5 PL spectra of the pure BiOBr, and Bi_2S_3/BiOBr heterostructure with the excitation wavelength of 310 nm.

Fig. 6 (A) photoreduction efficiency of Cr(VI) as a function of time using different catalysts; (B) linear transform $\ln(C/C_o) = f(t)$ of Cr(VI) reduction kinetics curves; (C) First-order rate constant over different catalysts; (D) Cr 2p high resolution XPS spectra of Bi_2S_3/BiOBr hybrid after photocatalytic reduction of Cr (IV), (The error bars reflect the standard deviations)**.**

Fig.7 Time dependence of the UV–vis spectra in photocatalytic reduction of 50 mL various concentration of Cr(VI) solution in presence of 50 mg Bi_2S_3/BiOBr composite: 10 mg/L (A), 30 mg/L (B), 50 mg/L (C), photoreduction (%) of Cr(VI) under different amount of thiourea (D), photoreduction (%) of Cr(VI) at different pH values over Bi_2S_3/BiOBr hybrid structure (E).

Fig. 8 (A) photoreduction efficiency of Cr(VI) as a function of time using different concentrations of (TA); (B) linear transform $\ln(Ct/C_o) = f(t)$ of Cr(VI) reduction kinetics curves; (D) First-order rate constant in presence of different concentrations of (TA).

Fig. 9 The photocatalytic reduction reaction and charge transfer mechanism of the Bi_2S_3/BiOBr photocatalyst under visible light irradiation.

Fig. 10 Cycling runs on the heterojunction Bi_2S_3/BiOBr for the photocatalytic reduction of Cr(VI) under visible light irradiation(A), and the XRD patterns of Bi_2S_3/BiOBr hybrid structure before and after the fourth recycle (B).

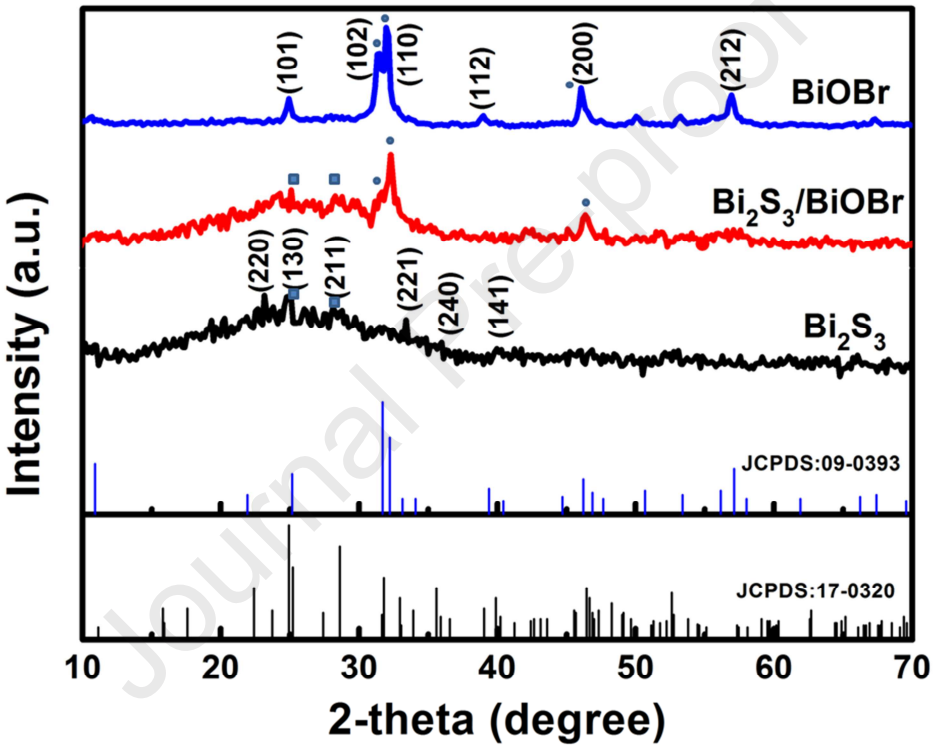

Fig. 1

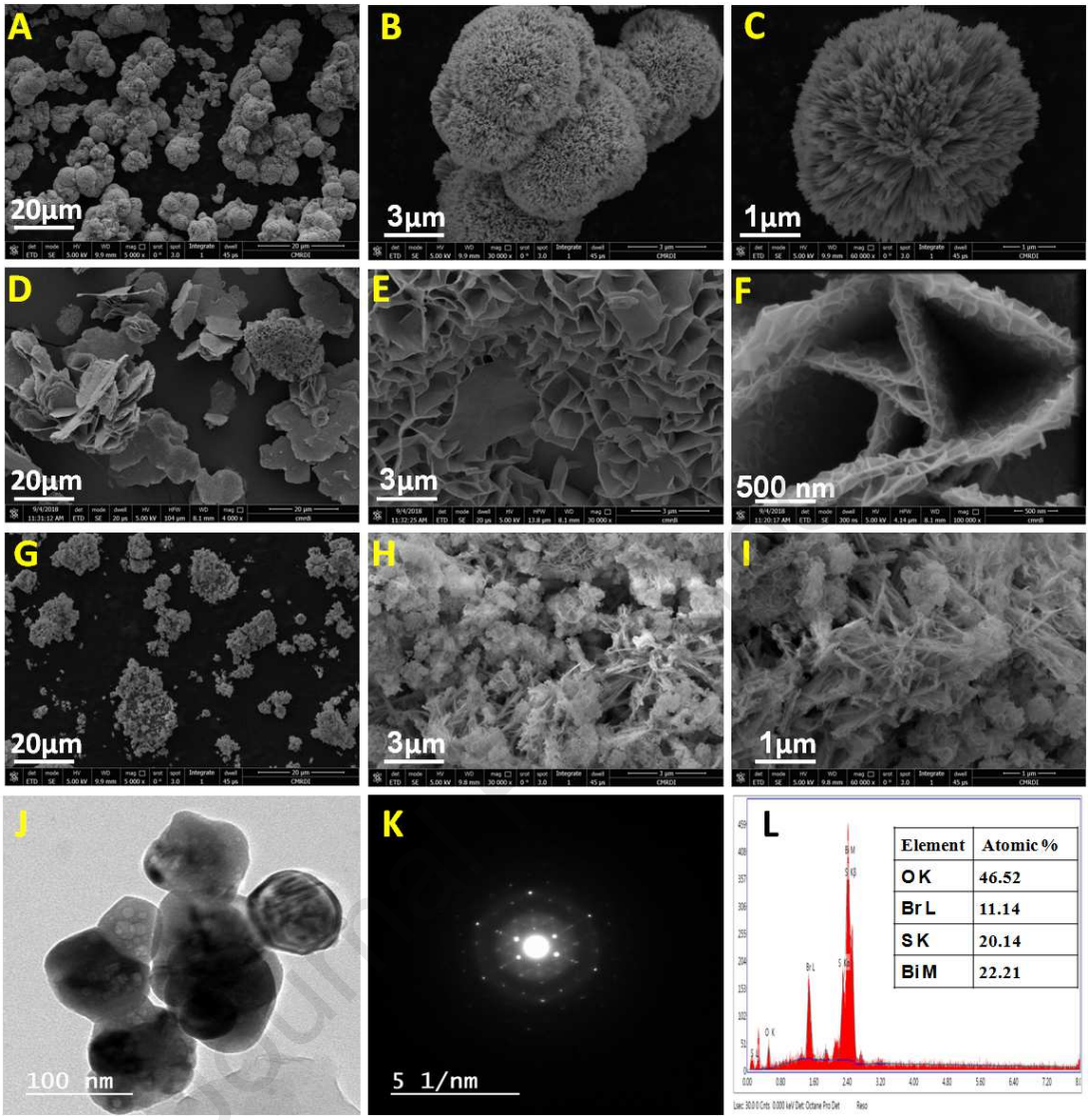
A
20µm
B
3µm
C
1µm
D
20µm
E
3µm
F
500 nm
G
20µm
H
3µm
I
1µm
J
100 nm
K
5 1/nm
L
Element | Atomic %
O K | 46.52
Br L | 11.14
S K | 20.14
Bi M | 22.21

Fig. 2

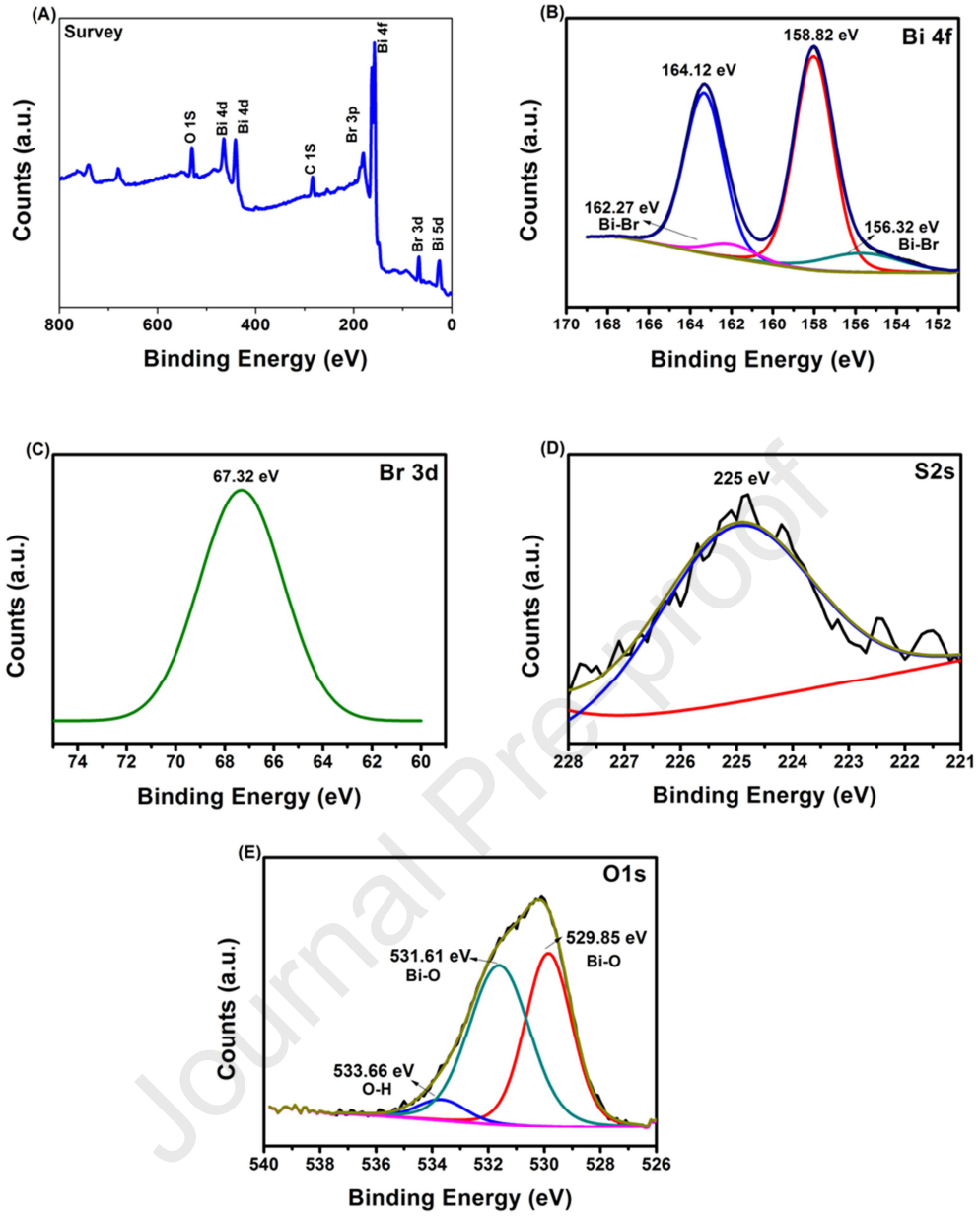

Fig. 3

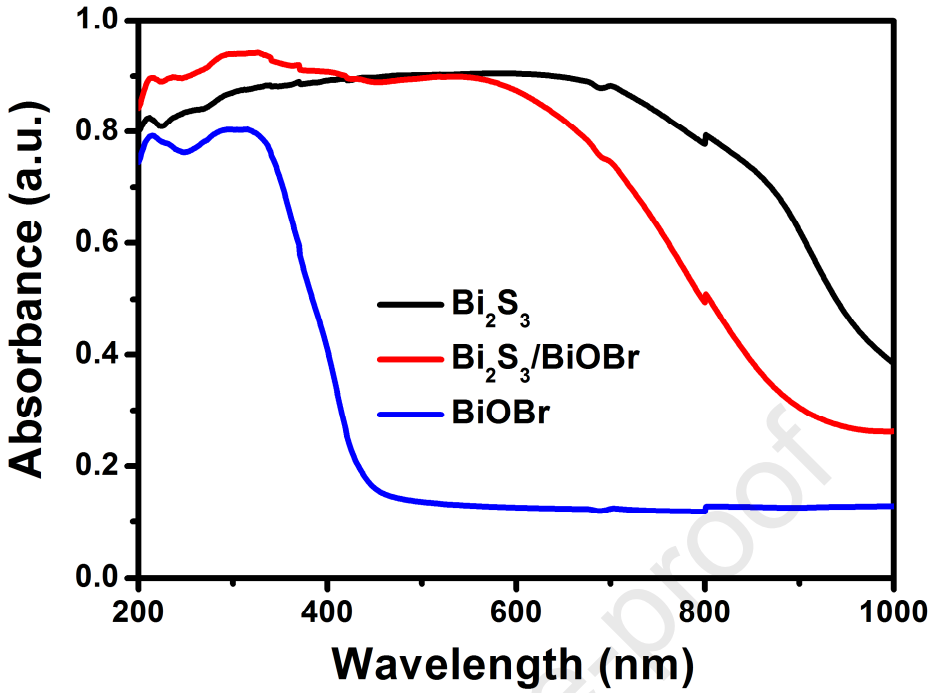

Fig. 4

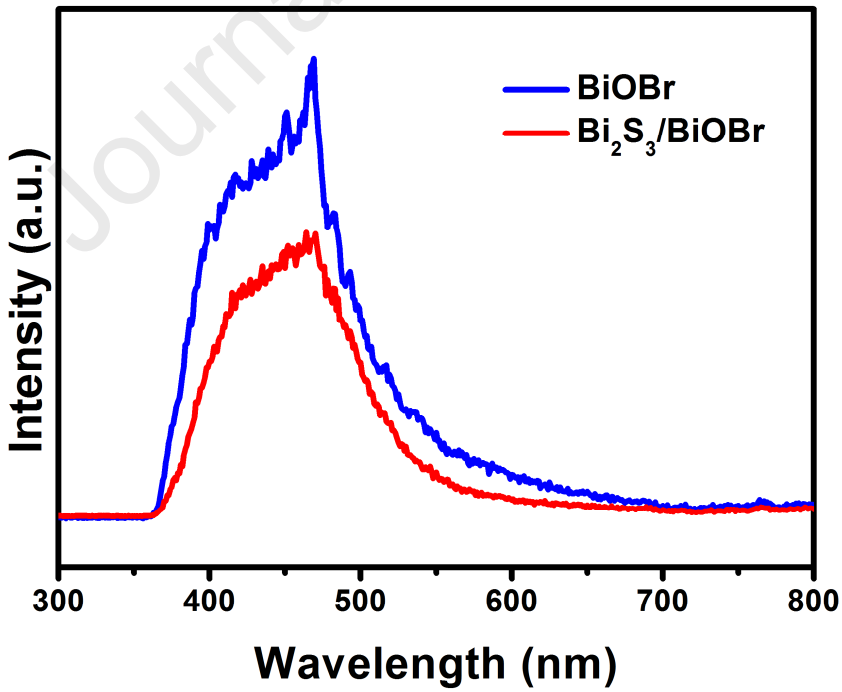

Fig. 5

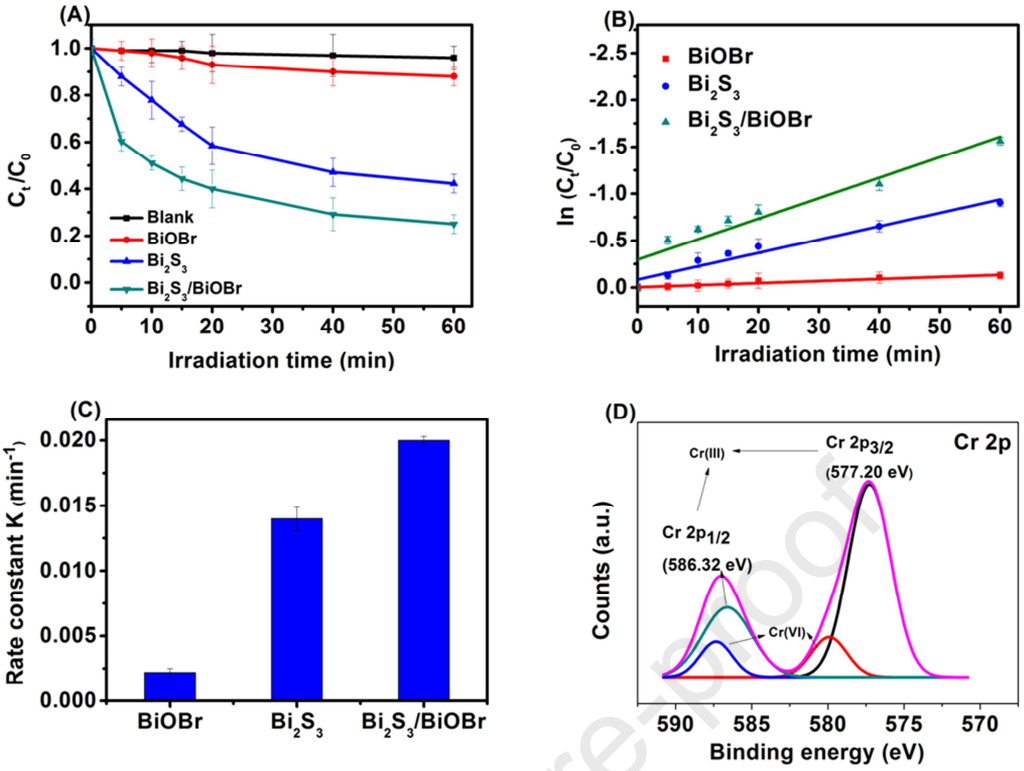

Fig. 6

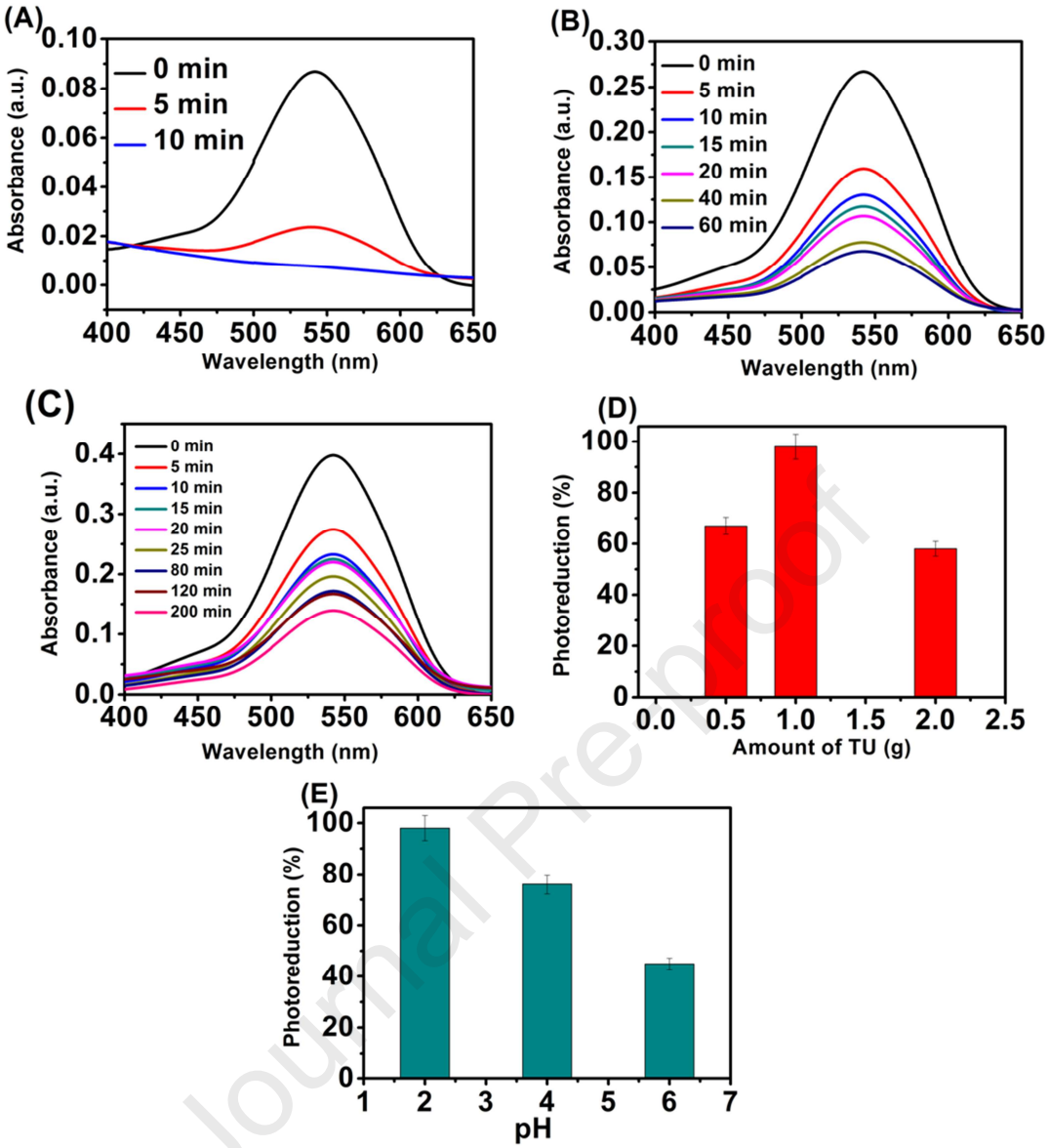

Fig. 7

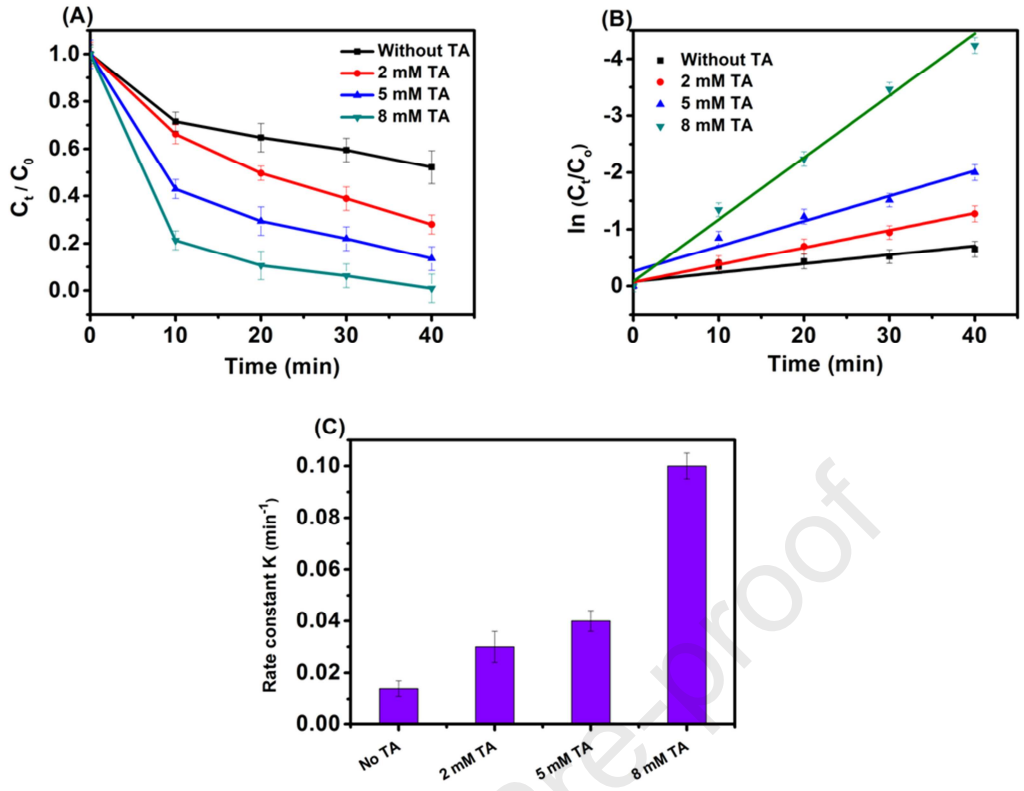

Fig. 8

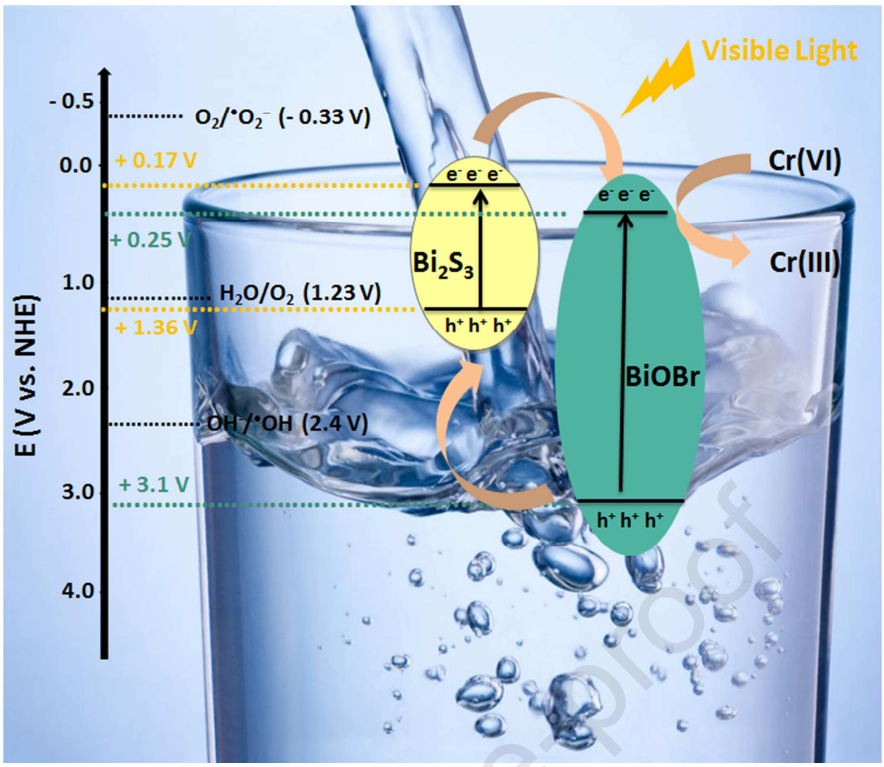

Fig. 9

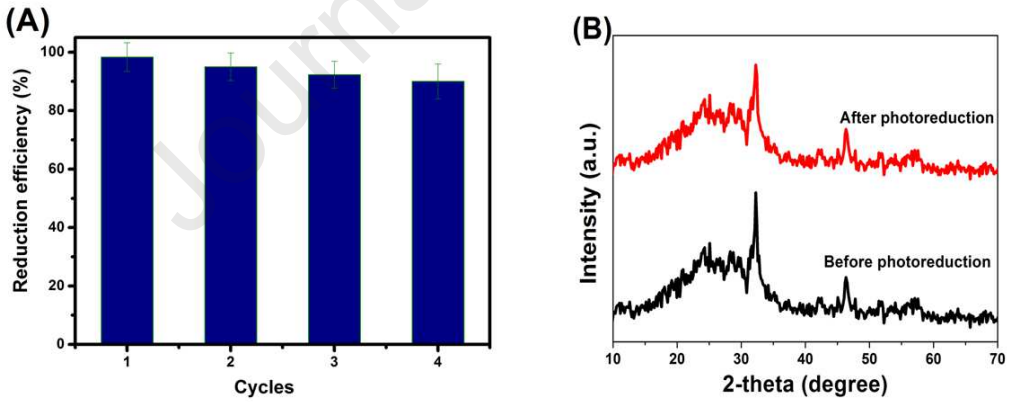

Fig. 10

Highlights

- A novel Bi_2S_3/BiOBr hybrid structure was developed by simple precipitation route.
- XPS analysis confirmed the complete reduction of Cr(VI) to Cr(III).
- Bi_2S_3/BiOBr exhibited rate constant of 10 times higher than that of BiOBr.
- Effect of tartaric acid, real sample test, and stability were studied.

Declaration of interests

☒ The authors declare that they have no known competing financial interests or personal relationships that could have appeared to influence the work reported in this paper.

☐The authors declare the following financial interests/personal relationships which may be considered as potential competing interests: